Case Studies in Construction Materials 15 (2021) e00726

Contents lists available at ScienceDirect

Case Studies in Construction Materials

journal homepage: www.elsevier.com/locate/cscm

Effects of fiber type and specimen thickness on flexural behavior of ultra-high-performance fiber-reinforced concrete subjected to uniaxial and biaxial stresses

Hyun-Oh Shin [a], Kyungteak Kim [a], Taekgeun Oh [b], Doo-Yeol Yoo [b,*]

[a] Department of Agricultural and Rural Engineering, Chungnam National University, 99 Daehak-ro, Yuseong-gu, Daejeon 34134, Republic of Korea
[b] Department of Architectural Engineering, Hanyang University, 222 Wangsimni-ro, Seongdong-gu, Seoul 04763, Republic of Korea

ARTICLE INFO

Keywords:
Ultra-high-performance fiber-reinforced concrete
Fiber type
Twist ratio
Thickness
Flexural performance
Stress state

ABSTRACT

In this study, we investigated the effects of steel fiber type and specimen thickness on the uniaxial and biaxial flexural behaviors of ultra-high-performance fiber-reinforced concrete (UHPFRC). For this purpose, three types of steel fibers (straight, three-times twisted, and six-times twisted) and three thicknesses of specimen (24, 48, and 72 mm) were used. The test results indicated that, owing to the larger perimeter of the triangular shape and mechanical anchorage effect, the twisted steel fibers exhibited better pullout resistance than the straight steel fiber with a circular shape, and its effectiveness increased with the number of ribs. In contrast, the best flexural behavior of UHPFRC was observed when the straight steel fiber was used under both uniaxial and biaxial stress states, and the six-times twisted steel fiber exhibited the worst flexural performance owing to the excessive bond strength of the composites. The uniaxial and biaxial flexural strengths of UHPFRC were insignificantly influenced by the sample thickness; however, the normalized toughness decreased with an increase in the thickness. A higher flexural strength, normalized toughness up to the peak, and deformability were observed under the biaxial flexural stress state than those under the uniaxial flexural stress state. The use of twisted steel fibers was more effective for slabs subjected to biaxial flexural stress than that for uniaxial beams.

1. Introduction

Ultra-high-performance fiber-reinforced concrete (UHPFRC), introduced in the mid-1990s [1], has been adopted as a novel building material worldwide [2]. Owing to its very high strength ($f_c^{'} \geq 150$ MPa [3], where $f_c^{'}$ is the compressive strength) and excellent ductility obtained by incorporating a high-volume content of steel fibers, UHPFRC can be used for fabricating informal structures, long-span bridge decks, and specially designed façades. A potential reason why these special applications cannot be realized using ordinary concrete is the difficulty of achieving thin cross-sections. Because conventional steel reinforcing bars or tendons are not required for nonstructural elements made of UHPFRC, their thickness can be substantially decreased by neglecting the thickness of the concrete cover. Thus, thin UHPFRC elements of various thicknesses are available and have been adopted in practice.

Recently, the size effect in UHPFRC elements has been studied by several researchers [4–7]. Spasojevic et al. [7] reported the presence of a size effect in UHPFRC beams, which is, however, clearly less significant than that in conventional fiber-reinforced and

* Corresponding author.
E-mail address: dyyoo@hanyang.ac.kr (D.-Y. Yoo).

https://doi.org/10.1016/j.cscm.2021.e00726
Received 9 August 2021; Received in revised form 30 September 2021; Accepted 4 October 2021
Available online 6 October 2021

Table 1
Chemical compositions of dry ingredients.

Composition [%]	PC	Silica flour	Silica sand	Silica fume
SiO_2	18.8	97.0	97.2	92.6
Al_2O_3	4.18	0.45	0.05	0.07
Fe_2O_3	3.72	0.1	0.13	0.49
CaO	65.3	0.07	0.13	0.67
MgO	2.43	0.01	0.01	1.8
SO_3	3.28	–	–	0.12
Na_2O	0.15	–	–	0.02
K_2O	1.1	–	0.02	1.13

[Note] PC = Type I ordinary Portland cement

ordinary concrete. The pseudo-plastic behavior of UHPFRC under tension limits the size effect on bending strength, and a higher strain capacity results in a smaller size effect [7]. Similarly, Mahmud et al. [6] found a minor size effect on the nominal flexural strength of UHPFRC beams up to 150-mm depth due to its high ductility. In contrast, Nguyen et al. [4] reported a clear size effect on the flexural strength, normalized deflection, and toughness of UHPFRC beams and indicated that a lower tensile ductility leads to a higher sensitivity to the specimen size. In addition, Yoo et al. [5] observed a clear decrease in flexural strength and normalized toughness owing to the increase in the cross-sectional sizes of UHPFRC beams under the size effect. They [5] recommended the use of longer steel fibers with higher aspect ratios to reduce the sensitivity to the size effect compared with shorter steel fibers and indicated that if the fiber distribution characteristics are controlled consistently regardless of the beam size, an insignificant size effect on flexural strength can be achieved for 2% by volume of steel fibers. This indicates that one of the main causes of the size effect in UHPFRC beams is the different fiber orientation and dispersion resulting from the different flow-velocity gradients.

Likewise, most previous studies [4–7] on the size effect in UHPFRC elements have focused on uniaxial elements. Kim et al. [8] noted that flexural properties of fiber-reinforced cement composites are dependent on the stress state, and the size effect on the biaxial tensile strength of concrete was stronger than the uniaxial tensile strength, according to Zi et al. [9]. The size effect is frequently used for bridge decks or slabs under biaxial flexural stress states [10,11], and the fiber orientations are also evidently affected by the casting method and flow direction [12,13]. Barnett et al. [13] noted that UHPFRC panels poured from the center are significantly stronger than others poured at the corner or randomly because the fiber alignment results in more fibers bridging the radial cracks. Yoo et al. [12] reported that the panels with concrete placed at the center (maximum moment region) exhibit better flexural performance than those with concrete placed at the corner, because of better fiber alignment and the presence of more fibers across the crack surfaces in the maximum moment region. Although an identical casting method is adopted, the fiber orientation characteristics can differ according to the panel size, especially its thickness, owing to the different gradients of flow velocity caused by the friction between the fresh UHPFRC and the mold wall. However, we couldn't find any studies on the size effect in UHPFRC panels under biaxial flexural stress states yet.

Meanwhile, to further improve the tensile or flexural performance of UHPFRC, various deformed steel fibers (e.g., hooked-end, twisted, half-hooked, crimped, and curved) [14–18] have been adopted owing to their enhanced pullout resistance. Wille et al. [17] reported that a fiber volume fraction of 1% is sufficient to trigger the strain-hardening behavior in UHPFRC and that an excellent tensile performance with a tensile strength of 13 MPa and strain capacity of 0.6% can be achieved using only 1.5% twisted steel fibers with a low twist ratio. Kim et al. [15] developed a novel curvilinear steel fiber as a reinforcement of ultra-high-performance concrete (UHPC) and reported that its tensile strength and energy absorption capacity per unit volume (g-value) can be significantly increased up to 52% and 174%, respectively, by replacing the conventional straight steel fiber with a moderately curved steel fiber with a curvature (κ) of 0.04 mm^{-1}. Yoo et al. [14] extensively compared the pullout and tensile behaviors of UHPC reinforced with both straight and deformed steel fibers and concluded that the order of effectiveness in enhancing its tensile performance is long-straight steel fiber $>$ twisted steel fiber $>$ half-hooked steel fiber $>$ hooked-end steel fiber. Murali et al. [18] reported that hooked-end steel fibers can more effectively enhance the impact energy dissipation capacity than the crimped steel fiber at various contents of 0.5–2%. Synthetically, the twisted steel fiber is the most effective for UHPC among the currently available highly deformed steel fiber types. In addition, its effectiveness is influenced by the number of twists [17,19]; however, this topic has been studied relatively insufficiently and a twist ratio between 3 and 6 has not yet been investigated for use in UHPC. Yoo et al. [19] considered twist ratios ranging from 0 to 3 ribs, and Wille et al. [17] used a relatively higher twist ratio of 6–8 ribs and 16 ribs per fiber length of 30 mm. This indicates that the effect of intermediate twist ratios between 3 and 6 is worthy to be investigated for UHPC.

Since the specimen thickness potentially causes size effect and fiber orientation and dispersion variations, its impact on the uniaxial and biaxial flexural properties of UHPFRC needs to be evaluated. Accordingly, this study first investigates the effects of steel fiber type and specimen thickness on the flexural behaviors of UHPFRC under both uniaxial and biaxial flexural stress states simultaneously, given a constant fiber volume fraction of 2%. For this purpose, three types of steel fibers, i.e., straight and twisted steel fibers with twist ratios of 3 and 6 ribs, and three specimen thicknesses of 24, 48, and 72 mm were considered for the uniaxial beams and biaxial panels made of UHPFRC to consider the stress state effect.

Table 2
Mix proportion of UHPC.

W/B	Mix design [kg/m^3]					
	Water	Cement	SF	Silica flour	Silica sand	SP*
0.2	160.3	788.5	197.1	236.6	867.4	52.6

[Note] UHPC = ultra-high-performance concrete, W/B = water-to-binder ratio, SF = silica fume, and SP = superplasticizer
*Superplasticizer includes 30% solid (= 15.8 kg/m^3) and 70% water (= 36.8 kg/m^3)

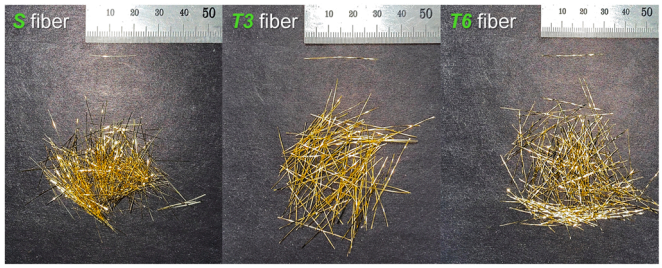

Fig. 1. Pictures of S, T3, and T6 fibers.

2. Test program

2.1. Materials and mix proportion

For creating a UHPC matrix, dry ingredients such as ordinary Portland cement (PC), silica fume (SF), silica flour, and silica sand were prepared. PC and SF, whose chemical compositions are listed in Table 1, were used as cementitious materials. The mean particle sizes of PC and SF were approximately 11.4 and 0.20 μm, respectively [19]. Silica flour was used as a filler and silica sand was used as a fine aggregate. Similar to SF, the major chemical component of was silicon dioxide (SiO_2); however, their chemical components were not reactive due to the coarse particle sizes [20] of approximately 6.8 and 236 μm, respectively. The detailed mix proportions of the UHPC are listed in Table 2. A low water-to-binder (W/B) ratio of 0.2 was used to achieve a very high compressive strength exceeding 150 MPa. To obtain a self-consolidating property, a polycarboxylate superplasticizer was added. A high-volume fraction of steel fibers is generally incorporated to achieve high ductility [21]. Therefore, 2% by volume of steel fibers was added in this study.

To investigate the influence of fiber type on the mechanical properties of UHPC, two types of steel fibers—straight (S) and twisted (T)—were used. The twisted steel fiber was divided into two categories based on the number of ribs (i.e., 3 and 6): T3 and T6 indicate twisted steel fibers with three and six ribs, respectively. The straight steel fiber has a diameter of 0.2 mm and a length of 19.5 mm, while the twisted steel fibers have a nominal diameter of 0.3 mm and a length of 30 mm. Fig. 1 shows the steel fiber types used in this study.

First, all dry ingredients were added in a Hobart-type mixer and premixed for 10 min. Then, water and superplasticizer were added and mixed for another 10 min. Once the mixture became flowable, it was used to produce dog-bone samples for single-fiber pullout as a fresh UHPC matrix. In addition, 2% steel fibers were carefully added and mixed for 5 min to fabricate a fresh UHPFRC mixture for the compressive and flexural tests.

2.2. Single-fiber pullout test

To evaluate the pullout resistance of the S, T3, and T6 fibers from the UHPC matrix, single-fiber pullout tests were conducted, similar to a previous study [22]. For this purpose, a small dog-bone sample with a cross-sectional area of 25 × 25 mm^2 was used [23]. Five dog-bone samples were fabricated for each variable to obtain reliable average results. A single steel fiber was initially fixed at the mold center by using a very thin PE film with an embedment length of 10 mm. The fiber was aligned in the direction of the pullout load. Fresh UHPC was then placed on one side (pull-out side) of the mold and cured in a laboratory room for 48 h. Subsequently, the other side of the mold was filled with a fresh UHPC mixture and cured for another 48 h. They were then demolded and immersed in a water tank at a high temperature of 90 °C for 72 h to promote strength development. Once the heat treatment was completed, the samples were removed from the water tank and placed in the laboratory until the testing date.

A universal testing machine (UTM) was used to pull out the fibers from the UHPC matrix. The applied force was measured from a load cell affixed to the test machine, whereas the fiber slip was measured from the movement of the grip under the assumption of negligible elastic deformations of the sample and grip. The fiber pullout test was complete when the recorded force reached zero. From the test results, the pullout load–slip curve could be obtained, and several important parameters such as the average bond strength, pullout work, equivalent bond strength, and maximum fiber tensile stress were calculated using equations provided elsewhere [22,24].

Fig. 2. Pictures of (a) uniaxial beams and (b) biaxial panels with various thicknesses of 24, 48, and 72 mm.

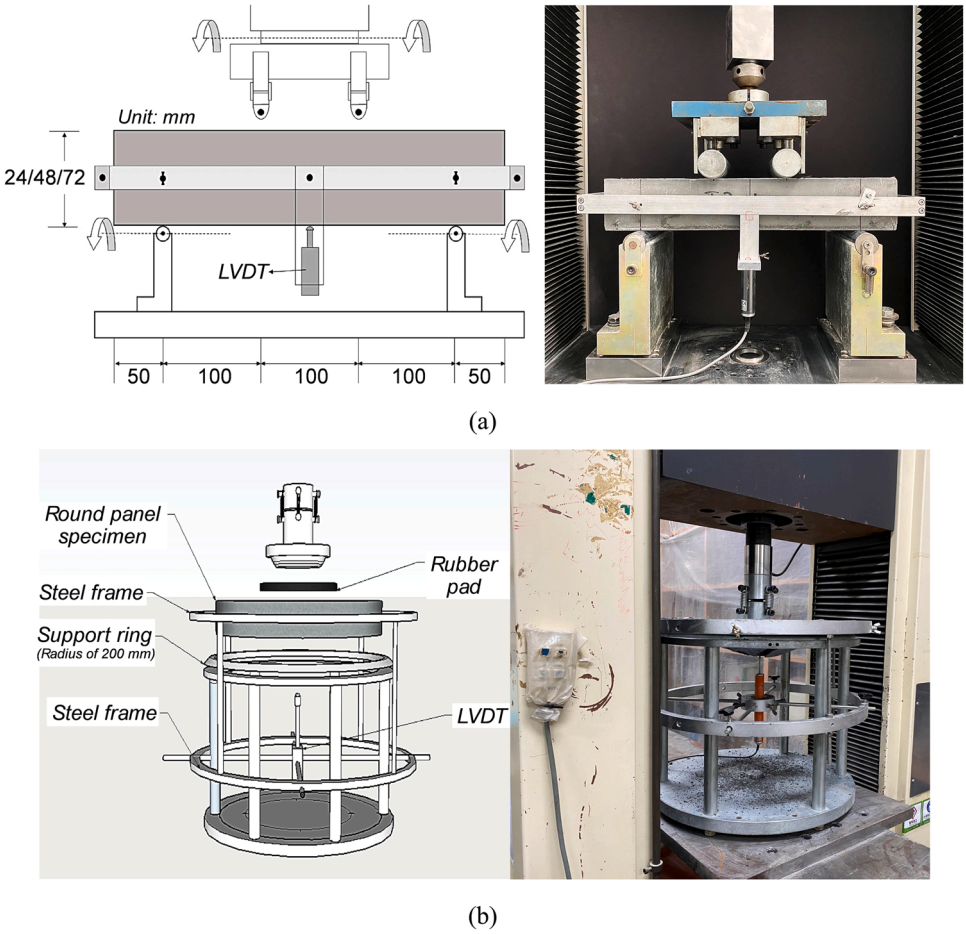

Fig. 3. Flexural test setup: (a) uniaxial four-point flexural test and (b) biaxial flexural test.

2.3. Compressive strength test

According to ASTM C39 [25], a cylindrical sample was fabricated and tested to measure the compressive strength. Three cylinders, each with a diameter of 100 mm and height of 200 mm, were used for each variable to obtain the average strength. In addition, to minimize the eccentric effect, the casting surface was ground using a diamond blade before testing. A uniaxial compressive force was monotonically applied by a UTM with a maximum capacity of 2000 kN at a loading rate of 2 kN/s. The applied force was measured from a load cell affixed to the machine and the compressive strength was calculated by dividing the peak load, P_{max}, by the cross-sectional area, A, as follows: $f_c^{'} = P_{max}/A$.

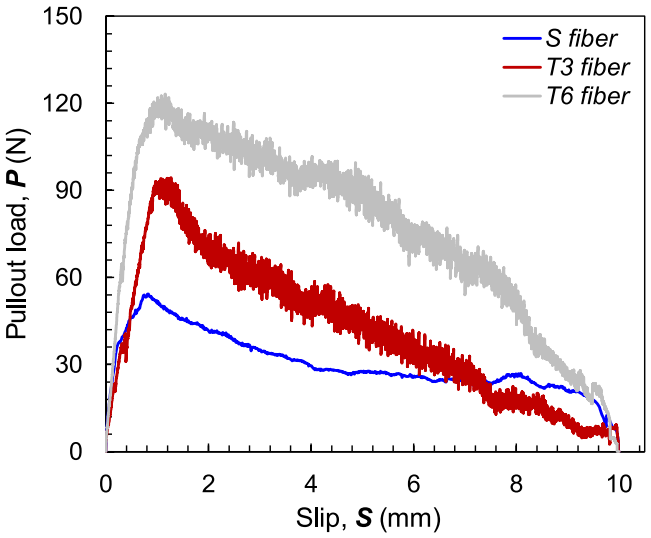

Fig. 4. Single fiber pullout load and slip curves.

2.4. Flexural tests

To evaluate the uniaxial flexural behavior of UHPC reinforced with various steel fibers, prismatic beams with various thicknesses such as 24, 48, and 72 mm were fabricated, as shown in Fig. 2a. Three beam samples were fabricated and tested for each variable to obtain the average results. To obtain better fiber alignment longitudinally and consistent results, they were cast in a direction parallel to the beam length [26]. Their width and length were 100 and 400 mm, respectively, and a 300-mm clear span length was adopted. A uniaxial load was applied by a UTM with a capacity of 200 kN at a rate of 1 mm/min, and the load and mid-span deflection were recorded through a load cell affixed and a linear variable differential transformer (LVDT). The uniaxial flexural test setup is shown in Fig. 3a.

Fig. 3b illustrates the biaxial flexural test setup of the UHPFRC panel, which is similar to the ISO 21022 recommendations [27]. The panels have a diameter of 420 mm and thicknesses of 24, 48, and 72 mm, identical to those of uniaxial flexural beams (Fig. 2b). Three panel samples were adopted for each variable. Loading and support rings with radii of 50 and 200 mm, respectively, were used. The maximum and uniform tensile stresses were obtained within the loading ring [28], which allowed the consideration of inhomogeneity of the material's strength. The uniaxial load was applied monotonically, load was measured from an affixed load cell, and pure center deflection was measured from the LVDT installed in an aluminum frame fixed to the panel. The 200-kN UTM was used for the biaxial flexural tests with sample thicknesses of 24 and 48 mm, while 500-kN UTM was adopted for the thickest (72 mm) panel due to its higher load carrying capacity. The loading rate of 1 mm/min was used equally for the biaxial flexural tests. Because of differential shapes of beam and panel, flow field characteristics were different (shear flow for uniaxial beam and radial flow for biaxial panel) [29]. Since the thicknesses of 24, 48, and 72 mm were equally applied for both the beams and panels, the size effect was not considered according to the specimen shape, given the identical thickness, similar to previous studies [8].

The uniaxial and biaxial flexural strengths were calculated based on the following equations.

$$f_u = \frac{P_{\max} L}{bh^2} \tag{1}$$

$$f_b = \frac{0.2387 P_{\max}}{t^2}\left[2(1+v)\ln\frac{R}{r} + \frac{(1-v)\left(R^2-r^2\right)}{R_0^2}\right] \tag{2}$$

where f_u is the uniaxial flexural strength, L is the span length, b is the beam width, h is the beam height, f_b is the biaxial flexural strength, t is the panel thickness, v is Poisson's ratio (0.2) for UHPC [30]), R is the radius of the support ring, r is the radius of the loading ring, and R_0 is the panel radius.

3. Test results and discussion

3.1. Fiber pullout behavior

Fig. 4 shows the comparative pullout load and slip curves of the S, T3, and T6 fibers from the same UHPC matrix. The average pullout parameters, calculated by Eqs. (3)–(6), are shown in Fig. 5.

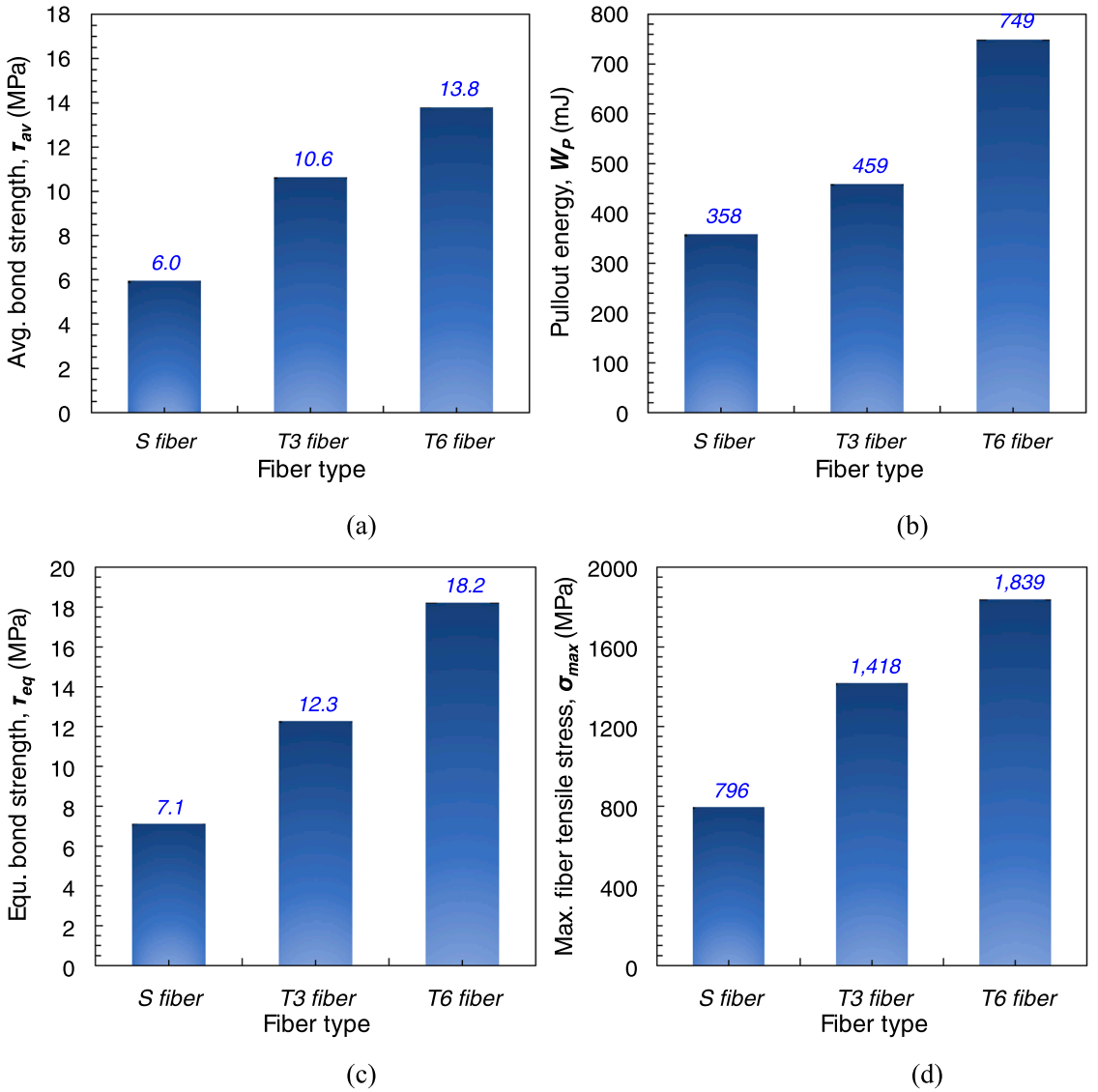

Fig. 5. Summary of pullout parameters: (a) average bond strength, (b) pullout energy, (c) equivalent bond strength, and (d) maximum fiber tensile stress.

$$\tau_{av} = \frac{P_{\max}}{\pi d_f L_E} \tag{3}$$

$$\sigma_{f,\max} = \frac{P_{\max}}{A_f} \tag{4}$$

$$W_P = \int_{s=0}^{s=L_E} P(s)ds \tag{5}$$

$$\tau_{eq} = \frac{2W_P}{\pi d_f L_E^2} \tag{6}$$

where, τ_{av} is the average bond strength, $P_{\max}$ is the maximum pullout load, d_f is the diameter of the fiber, L_E is the embedded length of the fiber, $\sigma_{f,\max}$ is the maximum tensile stress in the fiber, A_f is the cross-sectional area of the fiber, W_p is the pullout energy, s is the slip, and τ_{eq} is the equivalent bond strength.

Clearly, the twisted steel fibers (i.e., T3 and T6) provided higher average and equivalent bond strengths and pullout energy than the straight steel fibers. In addition, increasing the number of ribs was more effective in improving the pullout resistance of steel fibers

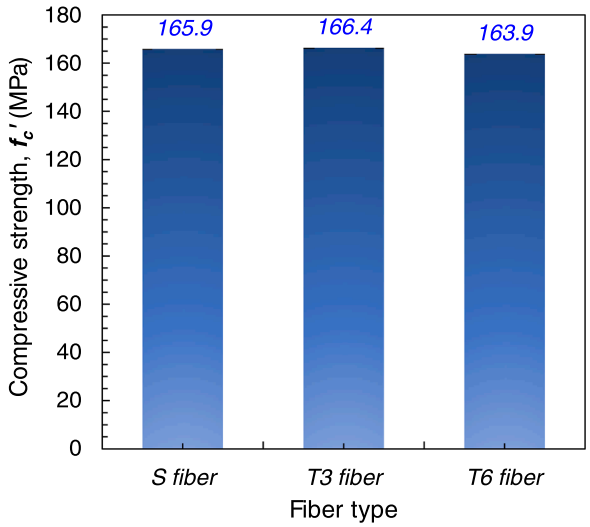

Fig. 6. Summary of compressive strengths.

from the matrix. For example, the highest average bond strength of 13.8 MPa was obtained for the T6 fiber sample, which is approximately 132% and 30% higher than those of the S and T3 fiber samples, respectively. This is due to the higher fiber intrinsic efficiency ratio (*FIER*) [31] and untwisting torque activated through the entire embedded length of the twisted steel fiber, which is consistent with the findings of Naaman [32], who reported that higher number of ribs result in better pullout resistance. The relative *FIER* of a triangular fiber to a circular fiber is 1.28 [31]; however, the T3 fiber leads to a 78% higher bond strength than the S fiber. This means that the mechanical anchorage effect can further increase the bond strength by increasing the untwisting torque. Thus, a higher number of ribs increased the pullout resistance more effectively. The maximum fiber tensile stress applied by the external pullout force was found to be 796 MPa for the S fiber case, and only 29% of its ultimate tensile strength was 2788 MPa [22]. In contrast, the maximum fiber tensile strengths of the T3 and T6 fibers significantly increased and the highest tensile strength of 1839 MPa was obtained, as shown in Fig. 5d. This indicates that the twisted steel fiber is more effectively used in terms of the strength margin of high-strength steel materials than straight steel fibers.

3.2. Compressive strength

The compressive strengths of all tested cylinders are shown in Fig. 6. They showed very high compressive strength, greater than 150 MPa, as recommended by the ACI committee 239 [3], which was insignificantly affected by the steel fiber type. For example, the highest compressive strength (166.4 MPa) was obtained for the T3 fiber sample, which was approximately 1.5% higher than the lowest strength (163.9 MPa) of the T6 fiber sample. This is consistent with the findings of several previous studies [33,34]. Yazıcı et al. [33] reported that the increase in compressive strength of concrete using fibers is relatively insignificant as compared to the tensile or flexural strength, and Kang et al. [34] noted that SF is the most significant factor affecting compressive strength, whereas the effects of fiber volume fraction and aspect ratio are relatively minor.

3.3. Uniaxial flexural behavior

3.3.1. Effect of beam thickness

Fig. 7 summarizes the flexural stress–deflection curves of all tested beams, and the flexural parameters, such as the flexural strengths at the limit of proportionality (LOP) and modulus of rupture (MOR) and normalized toughness, are listed in Fig. 8. The normalized toughness was calculated by an area under the flexural stress and normalized deflection (D/L) curve, where D is the deflection and L is the span length. Because of the addition of a high-volume fraction (2%) of steel fibers, all beams exhibited deflection-hardening behavior. By increasing the beam thickness from 24 to 72 mm, the bending stiffness increased in general, regardless of the fiber type, owing to the increased second moment of inertia, I, given an identical Young's modulus. For this reason, although an identical clear span length of 300 mm was adopted, the thinner beams provided the highest deflection capacity, which is the deflection corresponding to the maximum load, and decreased with an increase in the beam thickness. Naaman and Reinhardt [35] similarly reported the size effect in strain-hardening fiber-reinforced concrete and indicated that larger members yield smaller strain capacities, which are more sensitive to size than the post-cracking strengths. Because the strain capacity is related to deformability, their findings were consistent with the test results, as shown in Fig. 7. It has also been reported that a size effect of UHPFRC on flexural strength exists in the beam thickness range of 50–150 mm [4,5]. Nguyen et al. [4] noted that a higher tensile ductility provides less sensitivity to the size effect than the lower ductility, and Yoo et al. [5] explained the reason for the size effect in UHPFRC as different fiber distribution characteristics. Larger beams resulted in a more gradual gradient of flow velocity than smaller ones, causing poor

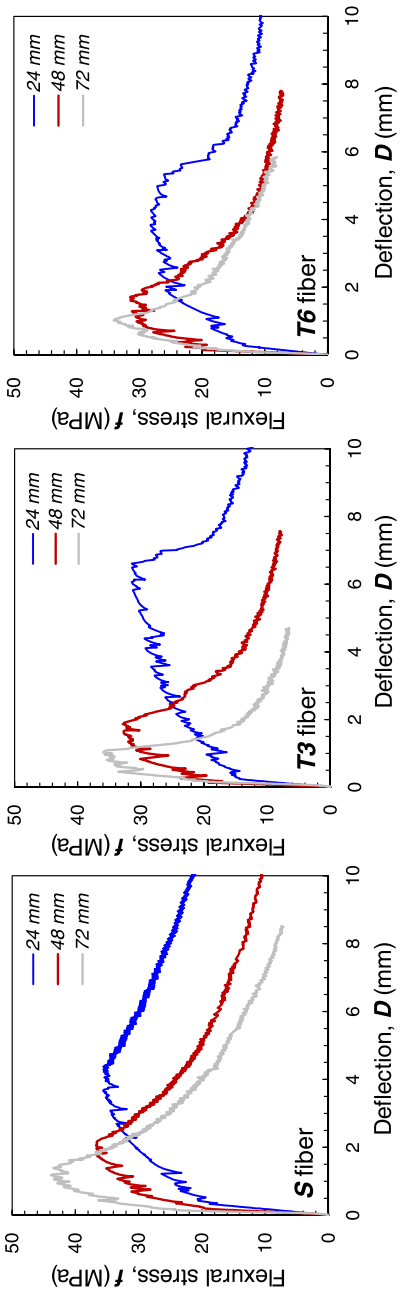

Fig. 7. Summary of uniaxial flexural stress and deflection curves.

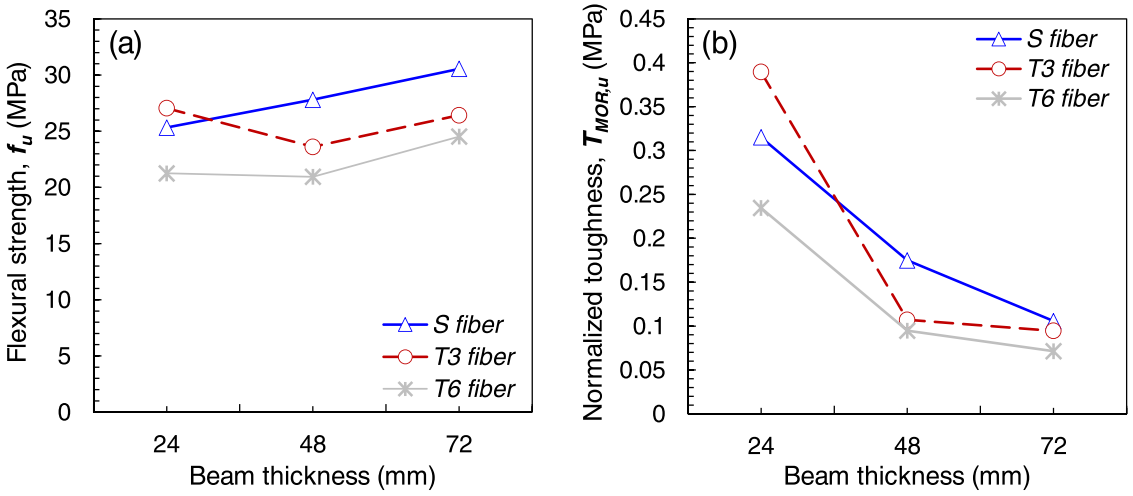

Fig. 8. Summary of uniaxial flexural parameters: (a) flexural strength and (b) normalized toughness.

fiber orientation and fewer fibers [5]. A higher beam width reduced the magnitude of torque, leading to a smaller magnitude of the drag force, so that more fibers become randomly oriented, resulting in a worse fiber orientation [5]. However, because an identical beam width of 100 mm was adopted in this study, the size effect on the fiber orientation might be limited. The insignificant size effect in UHPFRC beams verified the fact that the fiber distribution characteristics are similar [5]. In Fig. 8a, the flexural strength at the MOR (f_{MOR}) of UHPC beams reinforced with straight and twisted steel fibers was minimally influenced by a beam thickness of up to 72 mm. This indicates that the fiber orientation is well and consistently controlled to have a similar number of fibers at the crack surfaces. However, the normalized toughness, which is calculated based on the flexural stress-normalized deflection curve, was decreased by increasing the beam thickness, which is consistent with the findings of previous studies [4,5]. This is mainly because of the reduced deflection capacity, given a similar flexural strength, due to the increased bending stiffness. Thus, using a thin plate formed of UHPFRC is more effective in absorbing energy under flexure than that using a thicker beam formed of the same material.

3.3.2. Effect of steel fiber type

The pullout resistance of high-strength steel fibers in UHPC is mainly composed of interfacial friction and the anchorage effect through slight end deformation [36]. In contrast, the twisted steel fiber in UHPC provides untwisting torque through the entire embedment length and has higher *FIER* owing to its angular shape [37]. Thus, the twisted steel fiber led to much higher bond strength than that of the straight steel fiber in the same UHPC matrix [36]; however, it did not result in higher bridging strength in the composites [14]. To better understand the effect of the number of ribs in the twisted steel fiber on the flexural behavior of UHPC beams with various thicknesses, the flexural stress–deflection curves are compared in Fig. 7. In general, the S fiber samples provided a higher load-carrying capacity under flexure than the T3 and T6 fiber samples. Pyo et al. [38] reported that the thinner straight steel fiber with a diameter of 0.2 mm provides the higher tensile strength and energy absorption capacity (g) than the twisted steel fiber with a greater diameter of 0.3 mm, given an identical volume fraction of 2%, attributed to the higher number of fibers. Yoo et al. [14] also reported that the order of effectiveness in enhancing the post-cracking tensile performance of UHPC at the fiber volume fraction of 2% is as follows: long straight steel fiber > twisted steel fiber > short straight steel fiber > hooked-end steel fiber. This is attributed to the fact that, because of the insufficient matrix volume surrounding the fibers by the random orientation and inhomogeneous dispersion in the composites, the twisted steel fibers are prematurely pulled out with a splitting crack formation in the matrix. Tai et al. [39] reported that, radial and longitudinal micro cracks are formed along the length of the twisted steel fiber due to radial stresses caused by torsional moment. Thus, the bond strength of twisted fibers could not be completely developed in the composites, especially at the high fiber volume content of 2%. The flexural strength of UHPC was further decreased by increasing the number of ribs from 3 to 6, as shown in Fig. 8a, because of the excessive bond strength resulting from the untwisting torque. It has been recently reported that a single twisting of triangular steel fibers is effective in improving the flexural performance of UHPC and no further improvement with an increase of up to three times in the number of twisting is observed [19]. For instance, the highest flexural strength and normalized toughness of 27.8 and 0.17 MPa were obtained for the S fiber sample at a beam thickness of 48 mm, which were approximately 18% and 63% higher than those of the T3 fiber sample and 33% and 75% higher than those of the T6 fiber sample, respectively.

3.4. Biaxial flexural behavior

3.4.1. Effect of panel thickness

The biaxial flexural stress–deflection curves of all tested panels are summarized in Fig. 9. The shapes of the biaxial flexural stress and deflection curves were similar to those of uniaxial beams; however, the biaxial panels showed a higher deflection capacity than their counterparts. Due to the increased bending stiffness, the deflection capacity of the UHPFRC panels decreased with an increase in

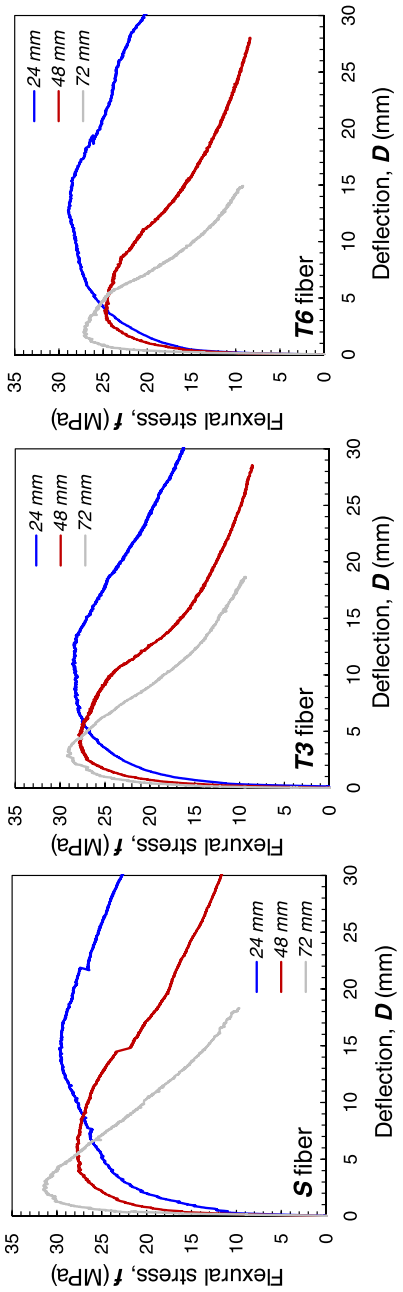

Fig. 9. Summary of biaxial flexural stress and deflection curves.

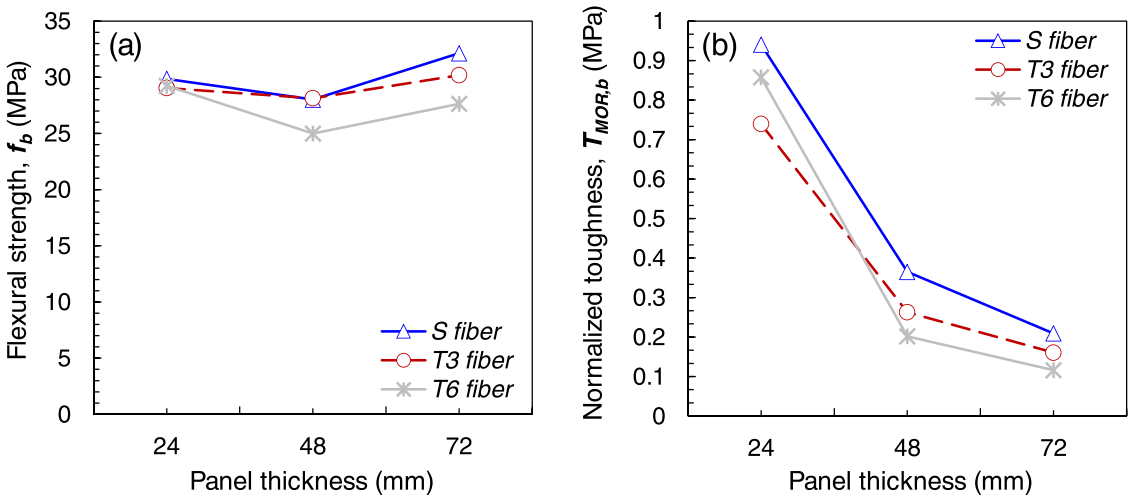

Fig. 10. Summary of biaxial flexural parameters: (a) flexural strength and (b) normalized toughness.

thickness. A steeper decrease in the flexural stress after reaching the peak was observed in the samples with twisted steel fibers, due to the surrounding matrix damages and premature pullout. Biaxial flexural parameters, such as the biaxial flexural strength calculated using Eq. (2) and the normalized toughness at the MOR point, are summarized in Fig. 10. The normalized toughness was calculated based on the biaxial flexural stress and normalized deflection ($D/2R$), where D is the mid-span deflection and R is the radius of the support ring. The biaxial flexural strength was also insignificantly influenced by the panel thickness, regardless of the fiber type (Fig. 10a), whereas the normalized toughness significantly decreased (Fig. 10b). These observations are coherent to the uniaxial flexural behavior of UHPFRC beams. Zi et al. [9] experimentally observed the strength reduction of a plain concrete panel under the biaxial flexural stress state owing to the size effect and noted stronger size effects under a biaxial flexural stress state than those under a uniaxial stress state. In contrast, Lepech and Li [40] reported that ECC shows much less sensitivity to the size effect on flexural strength than conventional reinforced concrete beams owing to its ductile nature. Yu et al. [41] also reported that the fracture-based size effect is negligible in ultra-high ductile cementitious composites, characterized by tension-hardening, and plasticity or viscoplasticity is more suitable for this material, moving itself to the horizontal region on the size effect curve. Therefore, although the size effect is a fundamental phenomenon in brittle materials such as concrete [42], very ductile materials exhibiting plastic behavior follow the strength criteria. For these reasons, the biaxial flexural strength of UHPFRC was insignificantly affected by a panel thickness of up to 72 mm. The strong size effect on the toughness is attributed to the fact that it was affected by both the strength and deflection capacity, which was reduced by the increased bending stiffness. The normalized toughness of UHPFRC at the MOR point was reduced by approximately 78–86% due to the increase of the panel thickness from 24 to 72 mm, regardless of the steel fiber type.

3.4.2. Effect of steel fiber type

Although the T6 fiber samples provided a smaller biaxial flexural strength than that of the S fiber samples, the biaxial flexural strength of the T3 fiber samples was quite similar to that of the S fiber samples (Fig. 10a). For example, the T3 and T6 fiber samples provided approximately 3% and 10% lower biaxial flexural strengths, respectively, than the S fiber sample on average. This indicates that the influence of the steel fiber type on flexural strength is relatively minor under the biaxial flexural stress state than that under the uniaxial stress state. However, even for the UHPFRC panels, the six-times twisted steel fiber (i.e., T6 fiber) exhibited the lowest strength owing to its excessive bond strength. Tai and El-Tawil [43] noted that twisted fibers cause more matrix damage with an increase in the inclination angle owing to the changed direction of the fiber force at the exit and its unique rib shape. Although we placed fresh UHPFRC at the panel center to control the fibers to be aligned vertically to the cracks, many fibers were inclined [12]. Thus, the twisted (T3 and T6) fibers potentially caused severe matrix damage and splitting cracks, which limited the further increase in the load-carrying capacity under biaxial flexure. The S fiber samples showed the optimum biaxial flexural performance in terms of strength and toughness compared with the T3 and T6 fiber samples, which is consistent with the uniaxial flexural behavior. For example, at a panel thickness of 72 mm, the highest biaxial flexural strength and normalized toughness were found to be 32.1 and 0.21 MPa, respectively, in the S fiber samples, which are approximately 6% and 30% higher than those of T3 fiber samples and 16% and 80% higher than those of T6 fiber samples.

3.4.3. Cracking behavior

The typical crack patterns of the tested panels and the number of cracks are shown in Fig. 11. The twisted steel fibers produced many more microcracks than the straight steel fibers in the same UHPC matrix up to the thickness of 48 mm, which is consistent with the findings of Wille et al. [17] and Yoo et al. [14]. Such a better cracking behavior of twisted steel fibers is attributed to their mechanical anchorage effect in addition to the interfacial frictional shear, leading to more effective stress transmission to the surrounding matrix than the straight steel fiber. For example, at a panel thickness of 24 mm, the numbers of cracks in the S, T3, and T6 fiber samples

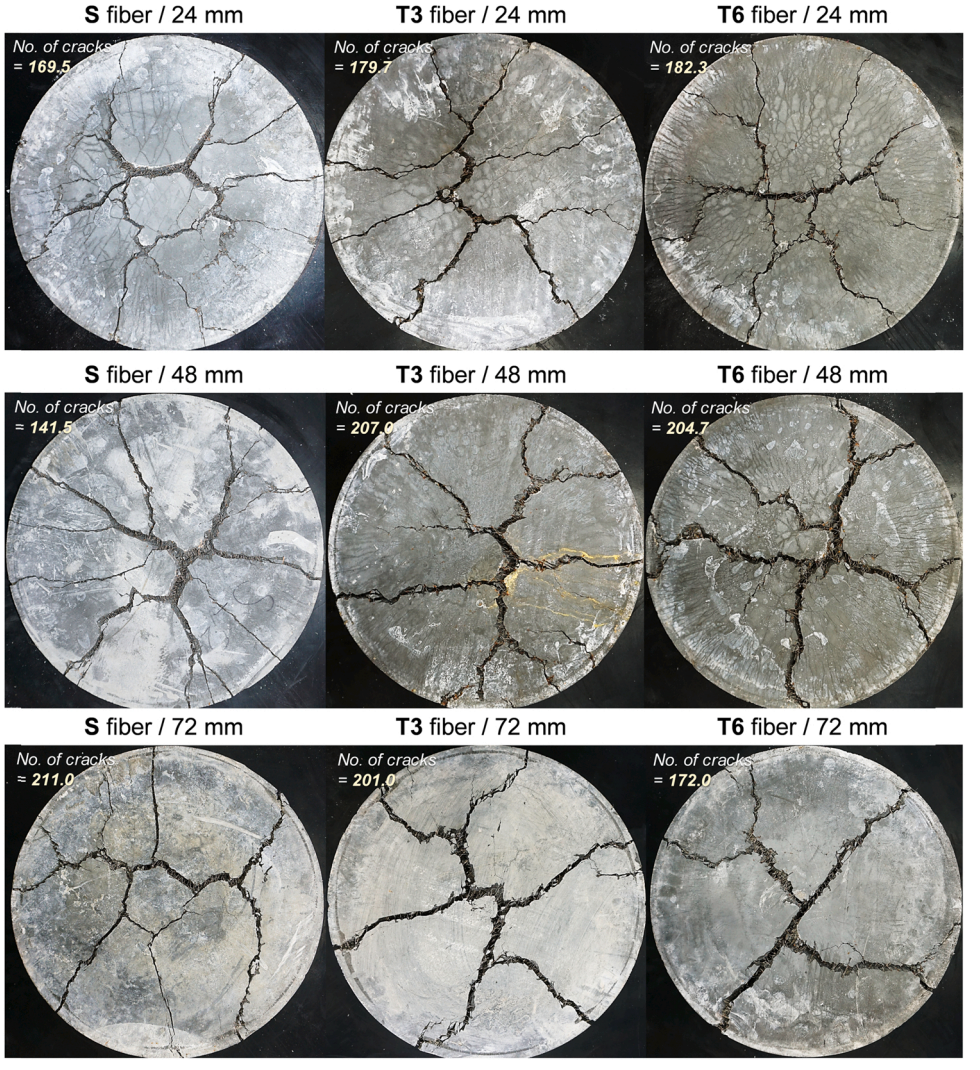

Fig. 11. Cracking behaviors of biaxial UHPFRC panels.

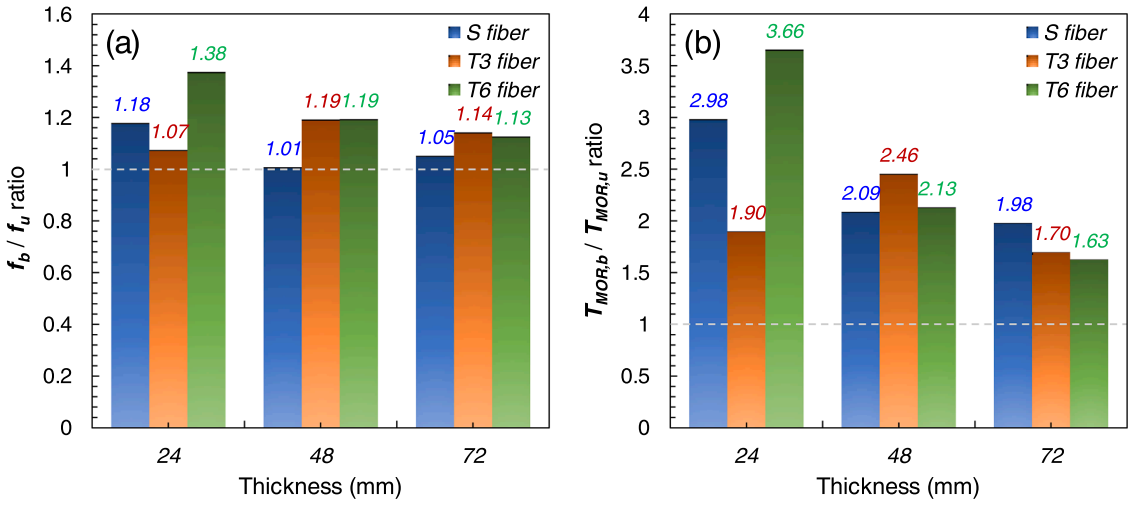

Fig. 12. Comparative ratios of (a) flexural strength and (b) normalized toughness under uniaxial and biaxial flexural stress states.

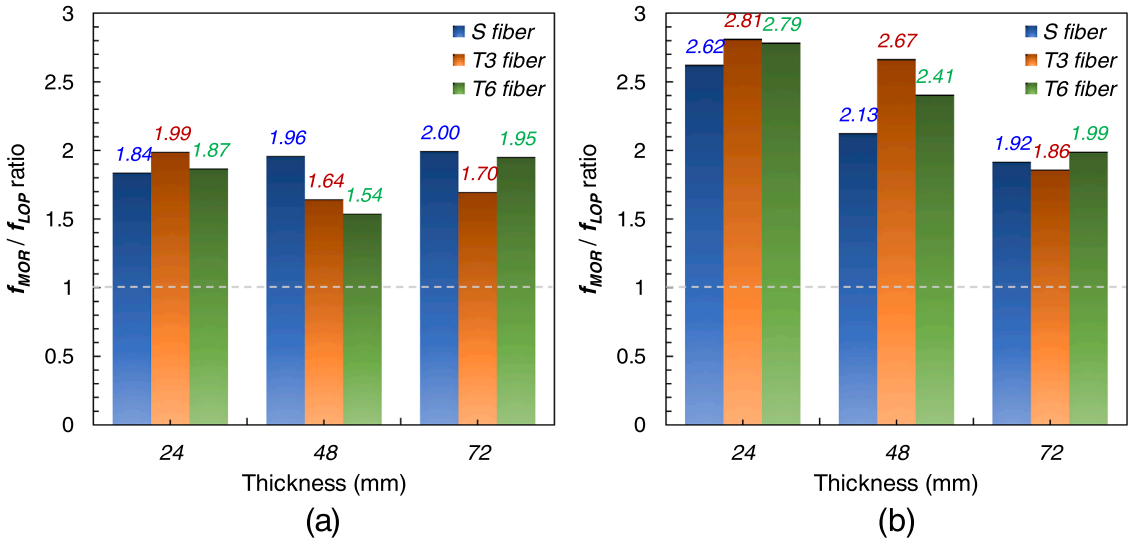

Fig. 13. Flexural strength ratios under (a) uniaxial flexure and (b) biaxial flexure.

were found to be 169.5, 179.7, and 182.3, respectively, The number of cracks in the UHPFRC panels seemed not to be influenced by the panel thickness. On the other hand, the S fiber sample produced more microcracks at the largest thickness of 72 mm, related to its best biaxial flexural performance in Fig. 11 in terms of the highest biaxial flexural strength and normalized toughness.

3.5. *Effect of stress state on the flexural behavior of UHPFRC*

The flexural strength and normalized toughness of UHPFRC under uniaxial and biaxial flexural stress states are compared in Fig. 12. Similar to the previous studies conducted by Kim et al. [8] and Shen et al. [44], a higher deformability was achieved in the UHPFRC panels than that in the beams. In addition, a higher flexural strength and normalized toughness up to the MOR point were observed for the panels under biaxial flexure than those for the uniaxial beams. This is because the panels provide higher values of fracture energy with multiple distributed cracks and more fibers with random orientation can withstand biaxial tensile stress than uniaxial stress [8]. Shen et al. [45] indicated earlier crack localization formation (about 63% of the ultimate strength) in the UHPFRC panels under an equi-biaxial flexural stress state than the uniaxial beams (about 90% of the ultimate strength) owing to the significant stress distribution by complex crack patterns with large crack surfaces. This was consistently observed in the present study. As shown in Fig. 13, the flexural strength ratio, f_{MOR}/f_{LOP}, was higher for the biaxial panels than that for the uniaxial beams, where f_{MOR} is the ultimate flexural strength, for example, f_u and f_b, and f_{LOP} is the initial cracking strength at the LOP. The differences in the f_{MOR}/f_{LOP} ratios were more apparent for the thinner sample cases. For example, a f_{MOR}/f_{LOP} ratio of 2.74 was found for 24-mm-thick UHPFRC panels on

average, which is approximately 44% higher than that of the 24-mm-thick UHPFRC beams. Thus, the biaxial flexural stress state easily induced the deflection-hardening behavior, relative to the uniaxial flexural stress state. The flexural strength ratio was insignificantly affected by the beam thickness under the uniaxial stress state, whereas it generally decreased with increasing panel thickness under a biaxial stress state. Based on a consideration of these post-cracking flexural performance, a thin slab or panel construction can be suitable UHPFRC applications. Furthermore, the twisted steel fibers (i.e., T3 and T6) showed higher flexural strength ratios than the straight steel fiber, which indicates that the use of twisted steel fibers in the UHPC matrix is more effective for slabs or panels where a biaxial stress state is applied than that for uniaxial members such as beams.

The normalized toughness ratios were evidently higher than the flexural strength ratios shown in Fig. 12, because they were influenced by both the strength and deflection capacity. The flexural strength ratio was not significantly affected by the sample thickness (Fig. 12a), whereas the normalized toughness ratio seemed to be influenced by the sample thickness (Fig. 12b). In general, a higher toughness ratio was obtained for thinner samples.

More than tenfold higher number of cracks were detected on the biaxial flexural panels, compared to the uniaxial flexural beams. For instance, the numbers of cracks in the panels reinforced with S, T3, and T6 fibers were found to be 13.2, 12.0, and 13.0 times higher than those in the beams with the same fiber types, given the sample thickness of 24 mm. The better cracking behaviors of UHPFRC under a biaxial flexural stress state than that under a uniaxial flexural stress state is related to the higher flexural strength ratio, causing an easier accomplishment of the deflection-hardening response. The complex crack patterns observed in the panels resulted from a significant stress redistribution after the crack formation, leading to the better flexural performance.

4. Conclusions

We investigated the influence of the steel fiber type on the uniaxial and biaxial flexural behaviors of UHPFRC with various thicknesses. The flexural parameters were also compared according to the stress state and the single-fiber pullout behavior was evaluated as basic data. Based on the test results and the above discussion, the following conclusions can be drawn.

1) The twisted steel fibers from the UHPC provided better pullout resistance than the straight steel fibers from the same matrix, and its effectiveness increased with the number of ribs increased from three to six.
2) The best uniaxial flexural performance of UHPFRC was observed when straight steel fibers were used compared with twisted steel fibers at the fiber volume fraction of 2%.
3) The flexural strengths of UHPFRC under uniaxial and biaxial stress states were insignificantly affected by the sample thickness up to 72 mm. In contrast, the normalized toughness significantly decreased with increasing the specimen thickness.
4) Better flexural behaviors, in terms of flexural strength, toughness, and deformability, were found under biaxial flexural stress than those under uniaxial flexural stress. The deflection-hardening behavior could be easily achieved when subjected to the biaxial flexural stress state.
5) Considering the post-cracking flexural performance, a thin slab or panel construction can be a suitable choice for UHPFRC application.
6) Using the twisted steel fiber was more effective for the slabs subjected to biaxial flexural stress than for uniaxial flexural stress.

Declaration of Competing Interest

The authors declare that they have no known competing financial interests or personal relationships that could have appeared to influence the work reported in this paper.

Acknowledgements

This work was supported by the National Research Foundation of Korea grant funded by the Korea government (MSIT) (No. 2019R1C1C1004784).

References

[1] P. Richard, M.H. Cheyrezy, Reactive powder concrete, Cem. Concr. Res. 25 (7) (1995) 1501–1511.
[2] D.Y. Yoo, Y.S. Yoon, A review on structural behavior, design, and application of ultra-high-performance fiber-reinforced concrete, Int. J. Concr. Struct. Mater. 10 (2) (2016) 125–142.
[3] ACI Committee 239. Ultra-high performance concrete. ACI Fall Convention. Toronto, Ontario, Canada; 2012.
[4] D.L. Nguyen, D.J. Kim, G.S. Ryu, K.T. Koh, Size effect on flexural behavior of ultra-high-performance hybrid fiber-reinforced concrete, Compos. Part B-Eng. 45 (1) (2013) 1104–1116.
[5] D.Y. Yoo, N. Banthia, S.T. Kang, Y.S. Yoon, Size effect in ultra-high-performance concrete beams, Eng. Fract. Mech. 157 (2016) 86–106.
[6] G.H. Mahmud, Z. Yang, A.M. Hassan, Experimental and numerical studies of size effects of Ultra High Performance Steel Fibre Reinforced Concrete (UHPFRC) beams, Constr. Build. Mater. 48 (2013) 1027–1034.
[7] Spasojevic A., Redaelli D., Fernández Ruiz M., Muttoni A. Influence of tensile properties of UHPFRC on size effect in bending. Second International Symposium on Ultra High Performance Concrete, Kassel, Germany, 2008, pp. 303–310.
[8] J. Kim, D.J. Kim, S.H. Park, G. Zi, Investigating the flexural resistance of fiber reinforced cementitious composites under biaxial condition, Compos. Struct. 122 (2015) 198–208.
[9] G. Zi, J. Kim, Z.P. Bazant, Size effect on biaxial flexural strength of concrete, ACI Mater. J. 111 (3) (2014) 319–326.

[10] M. Foglar, R. Hajek, J. Fladr, J. Pachman, J. Stoller, Full-scale experimental testing of the blast resistance of HPFRC and UHPFRC bridge decks, Constr. Build. Mater. 145 (2017) 588–601.
[11] E. Honarvar, S. Sritharan, J. Matthews Rouse, S. Aaleti, Bridge decks with precast UHPC waffle panels: a field evaluation and design optimization, J. Bridge Eng. 21 (1) (2016), 04015030.
[12] D.Y. Yoo, G. Zi, S.T. Kang, Y.S. Yoon, Biaxial flexural behavior of ultra-high-performance fiber-reinforced concrete with different fiber lengths and placement methods, Cem. Concr. Compos. 63 (2015) 51–66.
[13] S.J. Barnett, J.F. Lataste, T. Parry, S.G. Millard, M.N. Soutsos, Assessment of fibre orientation in ultra high performance fibre reinforced concrete and its effect on flexural strength, Mater. Struct. 43 (7) (2010) 1009–1023.
[14] D.Y. Yoo, S. Kim, J.J. Kim, B. Chun, An experimental study on pullout and tensile behavior of ultra-high-performance concrete reinforced with various steel fibers, Constr. Build. Mater. 206 (2019) 46–61.
[15] J.J. Kim, Y.S. Jang, D.Y. Yoo, Tensile properties of ultra-high-performance concrete improved by novel curvilinear steel fibers, J. Mater. Res. Technol.l 9 (4) (2020) 7570–7582.
[16] H. Zhang, T. Ji, X. Lin, Pullout behavior of steel fibers with different shapes from ultra-high performance concrete (UHPC) prepared with granite powder under different curing conditions, Constr. Build Mater. 211 (2019) 688–702.
[17] K. Wille, D.J. Kim, A.E. Naaman, Strain-hardening UHP-FRC with low fiber contents, Mater. Struct. 44 (3) (2011) 583–598.
[18] G. Murali, J. Venkatesh, N. Lokesh, T.R. Nava, K. Karthikeyan, Comparative experimental and analytical modeling of impact energy dissipation of ultra-high performance fibre reinforced concrete, KSCE J. Civil Eng. 22 (8) (2018) 3112–3119.
[19] D.Y. Yoo, I. You, G. Zi, Effects of waste liquid–crystal display glass powder and fiber geometry on the mechanical properties of ultra-high-performance concrete, Constr. Build. Mater. 266 (2021), 120938.
[20] I. You, G. Zi, D.Y. Yoo, D.A. Lange, Durability of concrete containing liquid crystal display glass powder for pavement, ACI Mater. J. 116 (6) (2019) 87–94.
[21] Graybeal BA. Material property characterization of ultra-high performance concrete (No. FHWA-HRT-06–103), Federal Highway Administration, Washington, D.C., 2006.
[22] D.Y. Yoo, S. Kim, Comparative pullout behavior of half-hooked and commercial steel fibers embedded in UHPC under static and impact loads, Cem. Concr. Compos 97 (2019) 89–106.
[23] M. Farooq, N. Banthia, FRP fibre-cementitious matrix interfacial bond under time-dependent loading, Mater Struct 52 (6) (2019) 1–11.
[24] D.Y. Yoo, B. Chun, J.J. Kim, Bond performance of abraded arch-type steel fibers in ultra-high-performance concrete, Cem. Concr. Compos. 109 (2020), 103538.
[25] ASTM C39, Standard Test Method for Compressive Strength of Cylindrical Concrete Specimens, ASTM International,, West Conshohocken, PA, 2020, pp. 1–8.
[26] S.T. Kang, J.K. Kim, The relation between fiber orientation and tensile behavior in an Ultra High Performance Fiber Reinforced Cementitious Composites (UHPFRCC), Cem. Concr. Res. 41 (10) (2011) 1001–1014.
[27] ISO 21022. Test method for fibre-reinforced cementitious composites–Load-deflection curve using circular plates. 2018, pp. 1–13.
[28] J. Kim, D.J. Kim, G. Zi, Improvement of the biaxial flexure test method for concrete, Cem. Concr. Compos. 37 (2013) 154–160.
[29] S.T. Kang, J.K. Kim, Numerical simulation of the variation of fiber orientation distribution during flow molding of ultra high performance cementitious composites (UHPCC), Cem. Concr. Compos. 34 (2) (2012) 208–217.
[30] H.G. Russel, B. Graybeal, Ultra-high performance concrete: a state-of-the-art report for the bridge community, FHWA-HRT 13–060 (2013) 1–176.
[31] A.E. Naaman, Engineered steel fibers with optimal properties for reinforcement of cement composites, J. Adv. Concr. Technol 1 (3) (2003) 241–252.
[32] A.E. Naaman, Fibers with slip-hardening bond. Third International Workshop on High Performance Fiber Reinforced Cement Composites (HPFRCC3), RILEM Publications,, Mainz, Germany, 1999, pp. 371–385.
[33] Ş. Yazıcı, G. İnan, V. Tabak, Effect of aspect ratio and volume fraction of steel fiber on the mechanical properties of SFRC, Constr. Build. Mater. 21 (6) (2007) 1250–1253.
[34] M.C. Kang, D.Y. Yoo, R. Gupta, Machine learning-based prediction for compressive and flexural strengths of steel fiber-reinforced concrete, Constr. Build. Mater. 266 (2021), 121117.
[35] A.E. Naaman, H.W. Reinhardt, Proposed classification of HPFRC composites based on their tensile response, Mater. Struct. 39 (5) (2006) 547–555.
[36] K. Wille, A.E. Naaman, Pullout behavior of high-strength steel fibers embedded in ultra-high-performance concrete, ACI Mater. J. 109 (4) (2012) 479–487.
[37] B. Chun, D.Y. Yoo, N. Banthia, Achieving slip-hardening behavior of sanded straight steel fibers in ultra-high-performance concrete, Cem. Concr. Compos. 113 (2020), 103669.
[38] S. Pyo, K. Wille, S. El-Tawil, A.E. Naaman, Strain rate dependent properties of ultra high performance fiber reinforced concrete (UHP-FRC) under tension, Cem. Concr. Compos. 56 (2015) 15–24.
[39] Y.S. Tai, S. El-Tawil, T.H. Chung, Performance of deformed steel fibers embedded in ultra-high performance concrete subjected to various pullout rates, Cem. Concr. Res. 89 (2016) 1–13.
[40] Lepech MD, Li VC. Preliminary findings on size effect in ECC structural members in flexure, In: Proceedings of the Seventh International Symposium on Brittle Matrix Composites. Warsaw, Poland, 2003, pp. 57–66.
[41] J. Yu, F. Dong, J. Ye, Experimental study on the size effect of ultra-high ductile cementitious composites, Constr. Build. Mater. 240 (2020), 117963.
[42] J. Suchorzewski, J. Tejchman, M. Nitka, J. Bobiński, Meso-scale analyses of size effect in brittle materials using DEM, Granul Matter 21 (1) (2019) 1–19.
[43] Y.S. Tai, S. El-Tawil, Computational investigation of twisted fiber pullout from ultra-high performance concrete, . 222 (2019) 229–242.
[44] X. Shen, E. Brühwiler, W. Peng, Biaxial flexural response of Strain-Hardening UHPFRC circular slab elements, Constr. Build. Mater. 255 (2020), 119344.
[45] X. Shen, E. Brühwiler, E. Denarié, W. Peng, An analytical inverse analysis to determine equi-biaxial tensile properties of strain-hardening UHPFRC from ring-on-ring test, Mater. Struct. 53 (5) (2020) 1–15.